Energy Proceedings
Vol 39, 2024
ISSN 2004-2965

Light-enhanced Catalyzed Hydrogenation of Gaseous CO_2 over Nanostructured Ni-Fe/$La_{0.8}Sr_{0.2}FeO_3$

Qiong Rao[1,2], Tianlong Yang[1,3], Jinrui Zhang[1,2], Yang Li[1,2], Zhongrui Gai[1,3], Ying Pan[1*]

1 Institute of Engineering Thermophysics, Chinese Academy of Sciences, Beijing 100190, China

2 University of Chinese Academy of Sciences, Beijing 100049, China

3 International Research Center for Renewable Energy & State Key Laboratory of Multiphase Flow in Power Engineering, Xi'an Jiaotong University, 710049, China

(*Corresponding Author: panying@iet.cn)

ABSTRACT

Global warming and climate change caused by greenhouse gas emissions have become urgent issues. Light-enhanced reverse water gas shift (RWGS) process is capable of efficiently converting CO_2 to CO at a low temperature with impressive rates by the $La_{0.8}Sr_{0.2}FeO_3$-supported Ni-Fe alloy (Ni-Fe/LSF). We test the reactivity of RWGS driven by pure thermal and photo-thermal coupled conditions in the same flow fixed-bed reactor. The results indicate that the apparent activation energy of RWGS reaction decreases by nearly 50% under direct light irradiation, and the CO production rate is enhanced by 2 times. In addition, the effects of light intensity on the reaction performance of CO_2 hydrogenation reaction and long-term stability are investigated. The formation of (Fe, Ni) phase is conducive to the high reactivity of the catalyst during long-term operation. By combining a suitable concentrating solar system, a matched photo-thermal reactor and optimizing the operating conditions, it is expected to achieve highly efficient CO_2 conversion at low temperatures through solar energy utilization.

Keywords: photothermal catalysis, CO_2 conversion, solar energy, reverse water gas shift, Ni-Fe/LSF

NONMENCLATURE

Abbreviations	
RWGS	reverse water gas shift
XRD	X-ray diffraction
SEM	scanning electron microscopy
DRS	UV-Vis diffuse reflectance spectra

1. INTRODUCTION

The continuous increase of CO_2 emissions has caused serious environmental problems and aroused widespread concern [1,2]. In recent years, considerable efforts have been made to realize the conversion of CO_2 into high value-added fuels or chemicals [3]. In particular, it is of great importance to catalyze the reverse water gas shift (RWGS) reaction ($CO_2 + H_2 \rightarrow CO + H_2O$) utilizing CO_2 hydrogenation technology to generate CO, which provide important raw materials for chemical production processes such as the Fischer-Tropsch process [4,5]. Currently, thermal catalytic RWGS reaction is mainly employed in industrial production to convert CO_2, whereas the process consumes large amounts of energy and causes some environmental problems [6]. Based on this, photothermal catalytic RWGS has been proposed to utilize solar energy to achieve more efficient and cleaner CO production, which is a promising approach to use CO_2 resources.

The catalysts suitable for photothermal RWGS reactions need to exhibit great stability, high activity and excellent photoresponsivity. However, it is a challenge to design a catalyst that meets all these criteria simultaneously. Noble metal catalysts have been extensively studied due to their intrinsic high catalytic activity and light-enhanced localized surface plasmon resonance effect [7–11]. Jia Jia et al. designed visible and near-infrared responsive Pd@Nb_2O_5 hybrid catalysts that achieved efficiently hydrogenates CO_2 to CO at an impressive rate as high as 1.8 mmol/g/h [12]. Yamashita and co-workers reported that Pt/H_xMoWO_y exhibited excellent catalytic performance (3.1 mmol/g/h) in the photothermal RWGS reaction [7]. Nevertheless, the

This is a paper for 15th International Conference on Applied Energy (ICAE2023), Dec. 3-7, 2023, Doha, Qatar.

expensive cost limits the potential for large-scale industrial applications of noble metal catalysts. To this end, researchers have conducted extensive studies on non-noble metal catalysts such as Cu and Fe [4,13–17]. Zhou Yang et al. found that Cu-CeO_2 catalyst showed a remarkable RWGS catalytic activity and CO selectivity, and the production of CO with light introduction has been significantly increased by 30% [15]. Ye et al. found that Fe nanoparticles loaded on Al_2O_3 showed excellent RWGS activity through a photothermal effect [13]. In addition, Fe catalysts coated with a carbon layer (Fe@C) exhibited superior catalytic performance in solar-driven RWGS with a nearly threefold increase in CO production rate compared to bare Fe nanoparticles [14]. Further, the researchers exploited the complementary and synergistic metal-metal interactions to develop catalysts with bimetallic structures. Different monometallic catalysts have various CO adsorption energy, affecting CO selectivity in the CO_2 hydrogenation reaction, and different monometallic catalysts have inconsistent strong absorption regions of light, which affects the efficiency of solar to fuels. The rational design of bimetallic catalysts utilizes metal-to-metal interfaces and metal-to-support oxide interfaces to modulate CO_2 and H_2 adsorption and dissociation activities, as well as full-spectrum solar energy absorption capacity [18,19].

In this work, a perovskite LSF-supported Ni-Fe bimetallic catalyst was developed for the photothermal RWGS reaction to realize the effective conversion of CO_2 at low temperatures. 10% Ni loading ratio was found to have optimal bimetallic synergistic catalytic effect. The perovskite LSF support with a large number of structural defects and oxygen vacancies is more favorable for CO production compared to Al_2O_3 and CeO_2. The effects of different reaction temperatures and light intensities on the reactivity of photothermal synergistic catalyzed RWGS were investigated. In addition, long-term stability tests were accompanied by a gradual enhancement of the activity. In conclusion, the results provide an efficient pathway for the conversion of greenhouse gas CO_2 to high value-added fuels by utilizing renewable solar energy.

2. EXPERIMENTAL SECTION

2.1 Catalyst preparation

The six catalysts studied in this work were prepared by sol-gel and mechanical mixing methods [20,21]. To obtain Ni-doped Fe oxides, the corresponding mass of $Fe(NO_3)_3{\cdot}9H_2O$ (Aladdin, 99.9%) and $Ni(NO_3)_2{\cdot}6H_2O$ (Aladdin, 99.99%) were dissolved to 30 mL dilute HNO_3 solution according to the stoichiometric ratio. After complete dissolution, citric acid (Aladdin, 99.5%) was added at a molar ratio of nitrate to citric acid of 1:2 and the solution pH was adjusted to 7 with ammonia (Aladdin, 25-28%). Subsequently, ethanol was added under vigorous stirring (molar ratio of nitrate to ethanol 1:2), then the clarified solution was introduced into a drying oven and kept at 230 °C for 1.5 h for solution concentration. The obtained precursor was heated at 600 °C for 3 h to remove organic residues, then calcined continuously at 1100 °C for 2 h and at 1260 °C for 4 h. To obtain LSF supports [22], stoichiometric ratios of $Sr(NO_3)_2$ (Aladdin, 99.5%), $Fe(NO_3)_3{\cdot}9H_2O$ (Aladdin, 99.9%), and $La(NO_3)_3{\cdot}6H_2O$ (Aladdin, 99%) were successively dissolved in 30 mL deionized water and stirred for 30 min at room temperature. Citric acid was then added to the solution at a molar ratio of citric acid to total cations of 3:1 and stirred magnetically at 50 °C for 30 min to form a chelating solution. Whereafter, ethylene glycol (Aladdin, 98%) at a molar ratio of 2:1 to citric acid was added to the chelating solution and magnetically stirred at 80 °C to promote gel formation. The acquired gel was dried at a constant temperature at 110 °C for 12 h, then roasted at 400 °C for 2 h to remove volatile components, and finally annealed in air at 800 °C for 4 h to form particles of the desired phase. The synthesized xwt%Ni-Fe_2O_3(x=0, 1, 10, 20) and LSF, as well as the commercially purchased nano-Al_2O_3 (Macklin, 99.99%, 40 nm) and nano-CeO_2 (Aladdin, 99.9%, 50 nm) were fully mechanically mixed in a molar ratio of 1:1.

2.2 Photothermal catalytic performance evaluation

The The RWGS reaction performance over the Ni-Fe/LSF was evaluated by a fixed-bed flow reactor at atmospheric pressure, as is shown in Fig. 1. Typically, about 30 mg catalyst was placed in the catalyst cup (6 mm diameter), at which point the sample thickness is about 1 mm, just enough to cover the thermocouple. Prior to the reaction, the catalysts were reduced at 500 °C for 40 min under H2 atmosphere. 2 mL/min CO_2 and 2 mL/min H_2 balanced with Ar into 30 mL/min in total were controlled by mass flow controllers and introduced into the reactor. The outlet gas was collected by gas bags, and then measured by gas chromatography (Agilent 8890) equipped with a thermal conductivity detector and a flame ionization detector. Under dark reaction conditions, the catalytic of RWGS activity was evaluated at 280-400 °C at 20 °C intervals. During the photo-thermal reaction process, light was introduced into the reaction system through a quartz window at the top of the reactor. A 300 W Xenon lamp (MC-PF300C), which

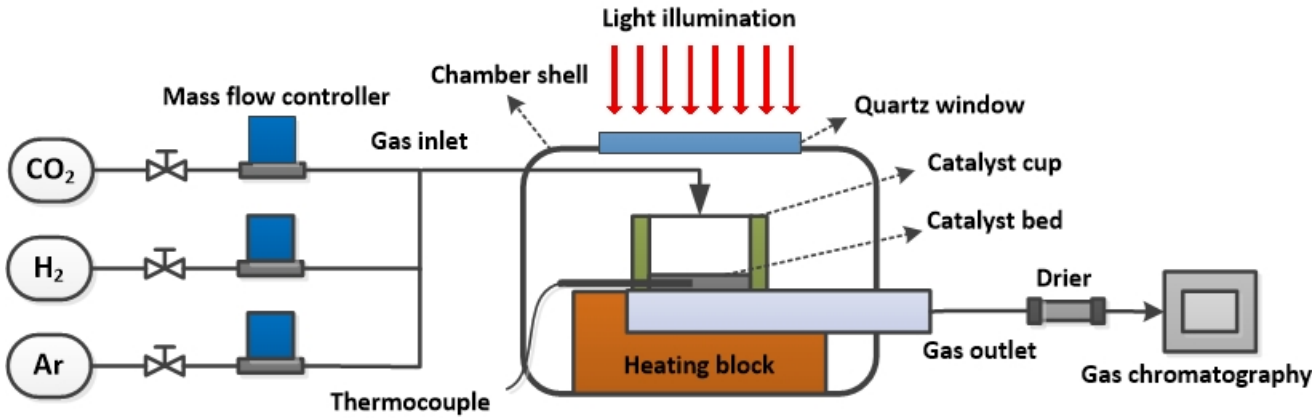

Fig. 1 Schematic diagram of gas phase photo-thermal catalysis fixed bed flow reactor.

has a spectral profile similar to the solar spectrum, is used as the light source.

2.3 Catalyst characterization

The X-ray diffraction (XRD) analysis of the catalysts was performed using the Bruker D8 advance powder X-ray diffractometer with Cu Kα irradiation (40 kV, 40 mA). The reflection angle, 2θ, was varied from 10 to 90° with a typical scan rate of 12 °/min. The morphological changes and elemental compositions of the prepared and cycled material were analyzed by scanning electron microscopy (SEM) coupled with energy dispersive X-ray spectroscopy (EDX) using a Zeiss MERLIN instrument. The optical properties of the catalysts were determined by UV-Vis diffuse reflectance spectra (DRS) using a UV-Vis spectrometer (Agilent Cary 7000).

3. RESULTS AND DISCUSSION

3.1 Material characterization

The xwt%Ni-Fe/LSF (x=0, 1,10,20) catalysts were successfully prepared by combining the sol-gel and mechanical mixing methods described in the experimental methods. Fig. 2 illustrates the XRD pattern of the catalysts pretreated with H_2. The diffraction peaks of the catalyst without Ni doping are in consistency with standard $La_{0.8}Sr_{0.2}FeO_3$ pattern (ICDD: 00-035-1480) and peaks corresponding to metallic Fe (ICDD: 03-065-4899). For 1wt%Ni-Fe/LSF, the peak corresponding to the metallic Ni is not present in the XRD spectra, which may have been due to the low Ni content and uniform dispersion of the prepared catalyst. The catalysts diffraction peaks appear tetrataenite ($Fe_{1.00}Ni_{1.00}$) (ICDD: 96-901-0018) when the Ni addition is higher than 10%, which indicates that Fe and Ni existed uniformly and stably in the catalysts.

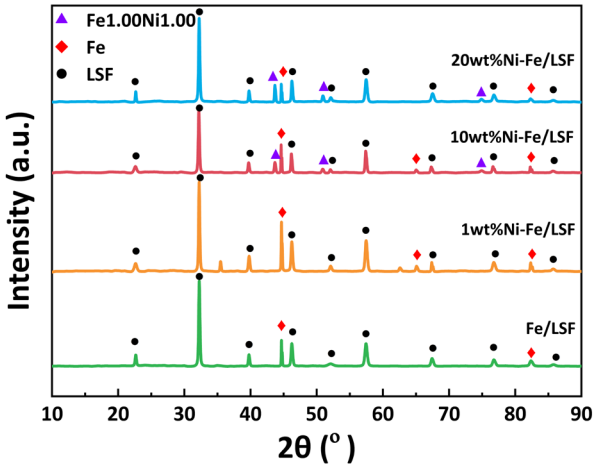

Fig. 2 XRD patterns of the fresh xwt%Ni-Fe/LSF (x=0, 1, 10, 20) samples.

The morphology and elemental distribution of xwt%Ni-Fe/LSF (x=0, 1,10,20) catalysts were observed by SEM and equipped EDS (Fig. 3). After the addition of Ni, the surface of the samples showed loose and porous. In general, the elemental distribution of the four catalysts is relatively uniform.

The light absorption capacities of catalysts were obtained by UV–Vis DRS as is shown in Fig. 4. Compared to Fe/LSF, the light absorption of the catalysts after loading with 1% and 10% Ni is significantly enhanced, especially in the ultraviolet and infrared region. when 20% Fe is replaced by Ni, the light absorption is improved (λ<470 nm), while the absorption effect is gradually weakened in 2200 nm>λ>470 nm spectral range. It is well known that higher intensity light absorption capacity facilitates the utilization of the solar spectrum in the photocatalytic processes and is more favorable for the subsequent catalytic processes [8].

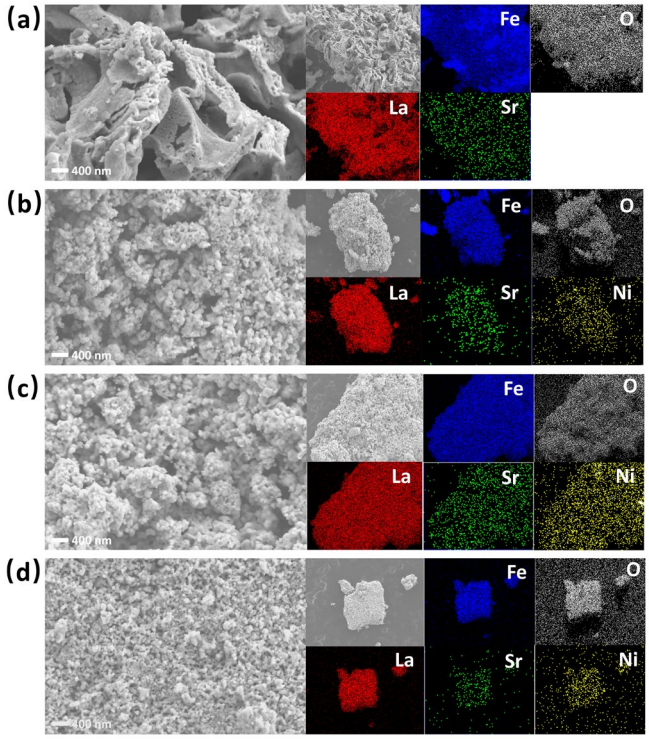

Fig. 3 SEM images and EDS mappings of the fresh (a) Fe/LSF, (b) 1wt%Ni-Fe/LSF, (c) 10wt%Ni-Fe/LSF, and (d) 20wt%Ni-Fe/LSF.

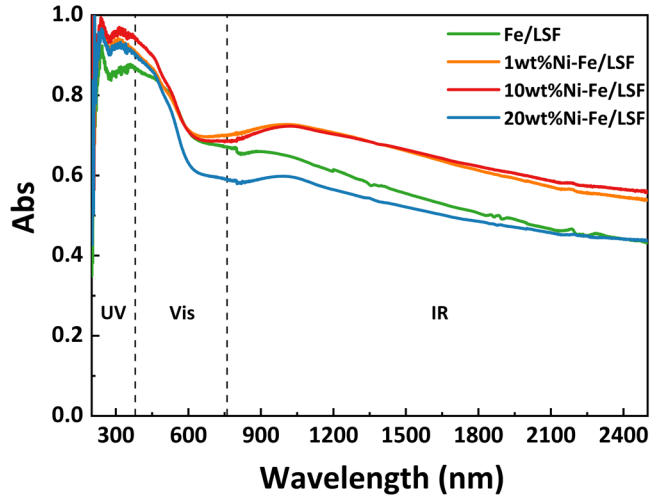

Fig. 4 DRS spectra of xwt%Ni-Fe/LSF (x=0, 1, 10, 20) catalysts.

3.2 *Effect of Ni doping ratio and supports on catalytic performance*

Fig. 5 demonstrates the catalytic performances of different Ni addition ratios and supports for the RWGS reaction at 320 °C with or without light irradiation. Due to the automatic thermal compensation mechanism of the reactor, the temperature of the catalyst did not change significantly under light irradiation, which confirms that the increase in activity under light irradiation is not caused by temperature changes. As shown in Fig. 5a, the performance of Fe/LSF is poor at only 4.47 mmol/g/h under dark condition. The RWGS activity of the catalyst is increased by 89.49% under irradiation (up to 8.47 mmol/g/h). The performance improved in catalysts doped with appropriate Ni content (10%) and is 4.83 mmol/g/h without light, whereas the activity improved 89.86% under illumination (up to 9.17 mmol/g/h). However, when 20% Ni is incorporated, the reaction performance decreased by 17.67% without light and 4.96% in the presence of light relative to no doping. The possible reason is that the addition of Ni exceeds a certain value, which leads to mutual sintering of metallic Fe and Ni, reducing the catalytic active site. It can be seen that the synergistic catalytic effect between Ni-Fe bimetals is strongest when the loading of Ni is 10%.

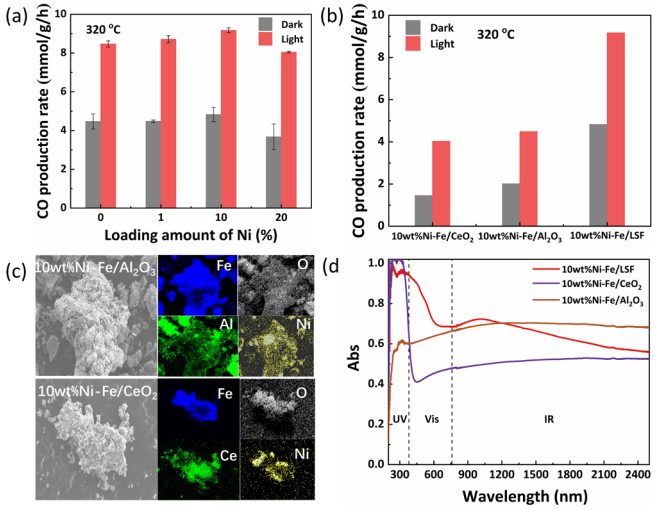

Fig.5. Catalytic performances of (a) xwt%Ni-Fe/LSF (x=0, 1, 10, 20) at 320 °C and (b) 10wt%Ni-Fe/LSF, 10wt%Ni-Fe/Al_2O_3, and 10wt%Ni-Fe/CeO_2. (c) EDS mappings of fresh 10wt%Ni-Fe/Al_2O_3 and 10wt%Ni-Fe/CeO_2. (d) DRS spectra of 10wt%Ni-Fe/LSF, 10wt%Ni-Fe/Al_2O_3, and 10wt%Ni-Fe/CeO_2 catalysts.

It can be seen that LSF support has more excellent catalytic activity for RWGS than nano-CeO_2 and Al_2O_3 as supports (Fig. 5b). Relative to 10wt%Ni-Fe/CeO_2 and 10wt%Ni-Fe/Al_2O_3, the Ni-Fe catalyst with LSF as the support increases the CO production rate by 233% for the dark reaction and 128% for the photo-thermal reaction. Fig. 5c and 5d illustrate the EDS mappings and DRS spectra of the Ni-Fe catalysts with different supports. The catalysts with CeO_2 and Al_2O_3 as supports showed obvious agglomeration of some elements and poor uniformity of element distribution, which is not conducive to maintaining high dispersion of catalytic sites on the surface. In addition, 10wt%Ni-Fe/CeO_2 exhibits high light absorption only in the UV range, but the spectral intensity in the UV band of the Xe lamp is only 5% of the full-wavelength intensity. For 10wt%Ni-

Fe/Al_2O_3, in the range of λ>1250 nm, its light absorption is slightly higher than that of 10wt%Ni-Fe/LSF, but the low energy of the long-wave infrared photons has a rather limited contribution to the reaction. In addition to the dispersion and light absorption capacity, the high defect degree and oxygen vacancy content characteristic of LSF perovskites can provide more active sites for CO_2 adsorption and conversion [15]. Based on these experimental results, 10wt%Ni-Fe/LSF catalyst is selected to further investigate the effect of light on CO_2 conversion.

3.3 Effect of temperature on catalytic performance

The temperature of the reaction was varied between 280 to 400 °C at constant pressure as shown in Fig. 6a. It is obvious that the activity of the catalyst is lower at lower temperature, and the photo-promoting activity of the catalyst is not apparent at the higher temperature. The rate enhancement (Light/Dark) decreases from 3.52 to 1.09 as the temperature increases from 280 to 400 °C. The result indicates that the dominant role of photons weakens with increasing temperature. The rate enhancement below 280 °C cannot be calculated because the catalytic activity under dark condition at this temperature is too poor to be detected by the gas chromatograph. The reaction rate versus temperature date is plotted in an Arrhenius plot as seen in Fig. 6b. The apparent activation energy for the RWGS reaction over 10wt%Ni-Fe/LSF catalyst decreases form 64.40 kJ/mol under dark condition to 35.07 kJ/mol with light. The reaction apparent activation energy decreases by nearly 83.63%, confirming that the introduction of weak light can greatly reduce the RWGS reaction energy barrier.

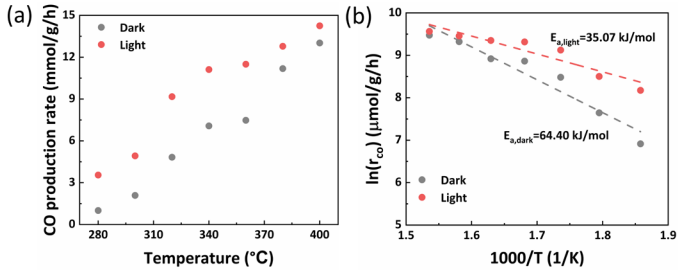

Fig. 6 Catalytic performances of 10wt%Ni-Fe/LSF at different reaction temperatures.

3.4 Effect of light intensity on catalytic performance

Fig. 7 demonstrates the variation of RWGS reactivity under different light intensities at uniform reaction temperature. The activity of RWGS reaction is improved approximately linearly with enhanced incident light intensity. Taking the pure thermal activity at the same temperature as the benchmark, the photo-thermal activity can be roughly attributed to the contribution of the thermal effect and light irradiation effect. At low irradiation intensity, the light-induced reaction efficiency accounts for 47.36%, and under elevated irradiation intensity, the percentage is gradually strengthened to 53.56%. It can be hypothesized that the light-induced promotion of activity diminishes when the light intensity exceeds a certain critical value, which is due to the absorption and utilization capacity of the catalyst with a fixed irradiation area is limited.

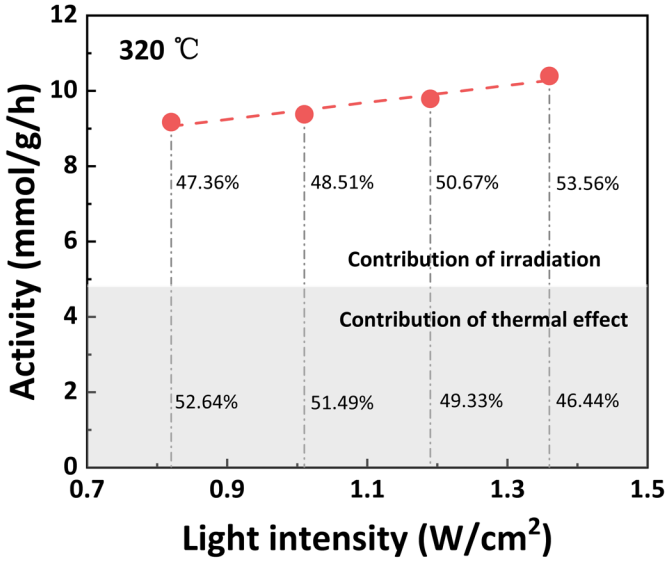

Fig. 7 The catalytic performances of 10wt%Ni-Fe/LSF evolution with light intensity.

3.5 Catalyst stability evaluation

Fig. 8 illustrates the long-term stability test results of the 10wt%Ni-Fe/LSF catalyst. With the continuous progress of the reaction, the photo-thermal RWGS maintains high reactivity, while the thermal RWGS activity shows gradually increasing trend. SEM image and EDS mapping of the catalyst after nearly 300 min continuous reaction are shown in Fig. 8b. Compared with the fresh sample, the surface morphology of the post-catalyst does not change significantly, and remains loose and porous with uniform distribution of the elements. Fig. 8c exhibits the XRD pattern of 10wt%Ni-Fe/LSF catalyst before and after the stability test. The diffraction peaks of the LSF support have no obvious change, while the $Fe_{1.00}Ni_{1.00}$ crystalline phase is transformed into (Fe, Ni) phase. The appearance of (Fe, Ni) substance may be the cause of the progressive enhancement in reactivity.

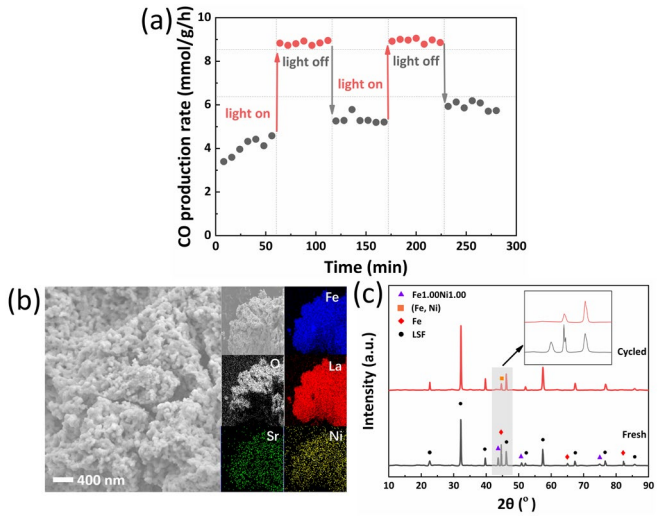

Fig. 8 The stability test of 10wt%Ni-Fe/LSF for RWGS reaction under light and dark conditions: (a) CO production rate, (b) SEM and EDS mapping of reacted catalyst, and (c) XRD patterns of fresh and reacted sample.

4. DISCUSSION

In conclusion, CO_2 hydrogenation reactions were investigated over Ni-Fe catalysts with different Ni addition ratios and supports under pure thermal and photo-thermal coupled reaction conditions. The results confirm that 10wt%Ni-Fe/LSF has excellent CO_2 conversion ability, the CO production rate reaches 4.83 mmol/g/h under pure thermal reaction, and up to 9.17 mmol/g/h coupled light irradiation. Under irradiation, the apparent activation energy calculated according to the Arrhenius formula is only nearly 1/2 that of the thermal reaction, proving that the introduction of light greatly reduces the reaction energy barrier. Long-term stability test observes gradual improvement in 10wt%Ni-Fe/LSF catalyst activity, which may be attributed to the formation of (Fe, Ni) phase. The findings provide an alternative pathway for utilizing solar energy to promote CO_2 conversion under mild reaction conditions.

ACKNOWLEDGEMENT

The authors would like to acknowledge the support by National Natural Science Foundation of China (NSFC) grant (No.52176026 and No. 52241601, No.51888103).

DECLARATION OF INTEREST STATEMENT

The authors declare that they have no known competing financial interests or personal relationships that could have appeared to influence the work reported in this paper. All authors read and approved the final manuscript.

REFERENCE

[1] Wang W, Himeda Y, Muckerman JT, Manbeck GF, Fujita E. CO_2 Hydrogenation to Formate and Methanol as an Alternative to Photo- and Electrochemical CO_2 Reduction. *Chem Rev* 2015.

[2] Fu J, Jiang K, Qiu X, Yu J, Liu M. Product selectivity of photocatalytic CO_2 reduction reactions. *Mater Today* 2020;32:222–43.

[3] Habisreutinger SN, Schmidt-mende L, Stolarczyk JK. Photocatalytic Reduction of CO_2 on TiO_2 and Other Semiconductors. *Angew Chemie Int Ed* 2013;52:7372–408.

[4] Gong J, Chu M, Guan W, Liu Y, Zhong Q, Cao M, et al. Regulating the Interfacial Synergy of Ni/Ga_2O_3 for CO_2 Hydrogenation toward the Reverse Water − Gas Shift Reaction. *Ind Eng Chem Res* 2021;60:9448–9455.

[5] Pham-huu C, Liu Y. Surface Oxygenate Species on TiC Reinforce Cobalt-Catalyzed Fischer−Tropsch Synthesis. *ACS Catal* 2021;11:8087–8096.

[6] Wang S, Tountas AA, Pan W, Zhao J, He L, Sun W, et al. CO_2 Footprint of Thermal Versus Photothermal CO_2 Catalysis. *Small* 2021;17.

[7] Ge H, Kuwahara Y, Kusu K, Kobayashi H, Yamashita H. Enhanced visible-NIR absorption and oxygen vacancy generation of Pt/HxMoWOy by H-spillover to facilitate photothermal catalytic CO_2 hydrogenation. *J Mater Chem A* 2022;10:10854–64.

[8] Ni W, Zeng M, Wang K, Lin Y, Zhang Z, Dai W, et al. Photo-thermal catalytic reverse water gas shift reaction over Pd/MaZrOx(M=Sr, SrMn) catalysts driven by "cycle-double sites." *J CO_2 Util* 2023;69:102413.

[9] Kobayashi D, Kobayashi H, Kusada K. Boosting reverse water-gas shift reaction activity of Pt nanoparticles through light doping of W. *J Mater Chem A* 2021;3:15613–7.

[10] Huber GW. Plasmon-enhanced reverse water gas shift reaction over oxide supported Au catalysts. *Catal Sci Technol* 2015;5:2590–2601.

[11] Martínez Molina P, Bossers KW, Wienk JD, Rohlfs J, Meulendijks N, Verheijen MA, et al. Sunlight Powered Continuous Flow Reverse Water Gas Shift Process Using a Plasmonic Au/TiO_2 Nanocatalyst. *Chem-An Asian J* 2023.

[12] Jia J, O'Brien PG, He L, Qiao Q, Fei T, Reyes LM, et al. Visible and Near-Infrared Photothermal Catalyzed Hydrogenation of Gaseous CO_2 over Nanostructured Pd@Nb_2O_5. *Adv Sci* 2016;3:1–13.

[13] Xianguang Meng, Tao Wang, Lequan Liu, Shuxin Ouyang, Peng Li, Huilin Hu, Tetsuya Kako, Hideo Iwai, Akihiro Tanaka and JY. Photothermal conversion of CO_2 into CH_4 with H_2 over Group VIII nanocatalysts an

alternative approach for solar fuel production. *AngewChem Int Ed* 2014;53:11478 –11482.
[14] Zhang H, Wang T, Wang J, Liu H, Dao TD, Li M. Surface-Plasmon-Enhanced Photodriven CO_2 Reduction Catalyzed by Metal–Organic-Framework-Derived Iron Nanoparticles Encapsulated by Ultrathin Carbon Layers. *Adv Mater* 2016;28:3703–10.
[15] Yang Z, Zeng M, Wang K, Yue X, Chen X, Dai W, et al. Visible light-assisted thermal catalytic reverse water gas reaction over Cu-CeO_2: The synergistic of hot electrons and oxygen vacancies induced by LSPR effect. *Fuel* 2022;315:123186.
[16] Feng K, Tian J, Guo M, Wang Y, Wang S, Wu Z, et al. Experimentally unveiling the origin of tunable selectivity for CO_2 hydrogenation over Ni-based catalysts. *Appl Catal B Environ* 2021;292.
[17] Wan L, Zhou Q, Wang X, Wood TE, Wang L, Duchesne PN, et al. Cu_2O nanocubes with mixed oxidation-state facets for (photo)catalytic hydrogenation of carbon dioxide. *Nat Catal* 2019;2:889–98.
[18] Bahmanpour AM, Signorile M, Kröcher O. Recent progress in syngas production via catalytic CO_2 hydrogenation reaction. *Appl Catal B Environ* 2021;295.
[19] Chen G, Waterhouse GIN, Shi R, Zhao J, Li Z, Wu L, et al. From Solar Energy to Fuels: Recent Advances in Light-Driven C1 Chemistry. *AngewChem Int Ed* 2019:17528–51.
[20] Chen YY, Guo M, Kim M, Liu Y, Qin L, Hsieh TL, et al. Predictive screening and validation on chemical looping oxygen carrier activation by tuning electronic structures via transition metal dopants. *Chem Eng J* 2021;406.
[21] Qin L, Guo M, Liu Y, Cheng Z, Fan JA, Fan LS. Enhanced methane conversion in chemical looping partial oxidation systems using a copper doping modification. *Appl Catal B Environ* 2018;235:143–9.
[22] Shafiefarhood A, Galinsky N, Huang Y, Chen Y, Li F. Fe_2O_3@$La_xSr_{1-x}FeO_3$ core-shell redox catalyst for methane partial oxidation. *ChemCatChem* 2014;6:790–9.